Published in final edited form as:
*Nat Struct Mol Biol*. 2016 July ; 23(7): 640–646. doi:10.1038/nsmb.3241.

# Direct observation of DNA threading in flap endonuclease complexes

**Faizah A AlMalki**[1,6], **Claudia S Flemming**[1], **Jing Zhang**[2,6], **Min Feng**[2,6], **Svetlana E Sedelnikova**[1], **Tom Ceska**[3], **John B Rafferty**[1,5], **Jon R Sayers**[2,4,5], and **Peter J Artymiuk**[1,6]

[1]Department of Molecular Biology and Biotechnology, University of Sheffield, Sheffield, UK

[2]Department of Infection, Immunology and Cardiovascular Disease, University of Sheffield, Sheffield, UK

[3]UCB Pharma, Bath Road, Slough, UK

[4]Florey Institute, University of Sheffield, Sheffield, UK

[5]Krebs Institute, University of Sheffield, Sheffield, UK

## Abstract

Maintenance of genome integrity requires that branched nucleic acid molecules are accurately processed to produce double-helical DNA. Flap endonucleases are essential enzymes that trim such branched molecules generated by Okazaki fragment synthesis during replication. Here, we report crystal structures of bacteriophage T5 flap endonuclease in complexes with intact DNA substrates, and products, at resolutions of 1.9–2.2 Å. They reveal single-stranded DNA threading through a hole in the enzyme enclosed by an inverted V-shaped helical arch straddling the active site. Residues lining the hole induce an unusual barb-like conformation in the DNA substrate juxtaposing the scissile phosphate and essential catalytic metal ions. A series of complexes and biochemical analyses show how the substrate's single-stranded branch approaches, threads



Correspondence should be addressed to J.R.S. (j.r.sayers@shef.ac.uk) or J.B.R. (j.rafferty@shef.ac.uk).
[6]Present Addresses: Department of Biology and Biotechnology, Taif University, Taif, KSA (F.A.A), MRC Weatherall Institute of Molecular Medicine, University of Oxford, Oxford OX3 UK (J.Z.), Cancer Therapeutics and Stratified Oncology, Genome Institute of Singapore, Agency for Science, Technology, and Research (A*STAR), Biopolis, Singapore (M.F.), deceased (P.J.A).

**Accession codes**

Coordinates and structure factors have been deposited in the Protein Data Bank under accession codes: PDB 5HMM (wt T5Fen); PDB 5HML (T5FenD153K); PDB 5HNK (T5FenD153K–5ov4 complexes C1 and C2); and PDB 5HP4 (T5FenD155K–3ov6, complex C3).

**Author Contributions**

J.R.S., T.C. and P.J.A. conceived the project. J.R.S. designed mutants and enzyme assays. M.F. and J.Z. carried out mutagenesis, biochemical experiments and kinetics analyses (supervised by J.R.S.). F.A.A., C.S.F., M.F. and J.Z. expressed proteins and together with S.E.S., purified them. F.A.A. carried out crystallization and data collection on complexes (C1–C3). C.S.F. carried out crystallization and data collection on wt and T5FenD153K variant. Structure refinement was carried out initially by F.A.A. and C.S.F, under supervision of J.B.R. and P.J.A., with final refinements by J.R.S. with input from J.B.R and T.C. All authors discussed the results and commented on the manuscript. P.J.A. made an initial draft of the manuscript. J.R.S. wrote the manuscript with input from all authors.

**Competing financial interests**

J.R.S. and J.Z. have filed intellectual property in the area of use of recombinant flap endonucleases. The University of Sheffield has a consultancy agreement with Atlas Genetics Ltd. in the area of flap endonuclease biology (J.R.S.). J.R.S holds equity in a company developing flap endonuclease inhibitors.


Europe PMC Funders Author Manuscripts

through, and finally emerges on the far side of the enzyme. Our studies suggest that substrate recognition involves an unusual “fly-casting, thread, bend and barb” mechanism.

## Introduction

Branched nucleic acid structures arise transiently in all cells undergoing DNA replication and repair. Flaps result from extension of short RNA primers laid down during Okazaki fragment formation on the lagging DNA strand. A 5′ flap structure is created as the growing 3′ end of the lagging strand approaches the 5′ end of the RNA primer used to initiate the previous Okazaki fragment in a process known as strand displacement synthesis1. These flap structures must be processed efficiently to yield ligatable nicks given that they are formed approximately every 150–1000 nucleotides on the lagging strand2,3. Flap endonucleases (FENs) are structure-specific metalloenzymes responsible for processing flap structures4,5. FENs are required by organisms as diverse as microorganisms and mammals: FEN activity is essential for viability in bacteria6–8; haplo-insufficient (*Fen*$^{-/+}$) mice show rapid tumor development while homozygous knockout animals lacking FEN1 entirely (*Fen*$^{-/-}$) die *in utero*9.

FENs cleave flap substrates even when 5′-single-stranded branches of up to ~200 nucleotides are present. Such observations prompted suggestions that the flap’s 5′ end threads through a hole in a doughnut-like FEN protein10. Subsequently, structural studies identified a hole in a flap endonuclease just wide enough to accommodate single-stranded DNA11, thus providing some physical evidence to support the threading hypothesis. However, Joyce and coworkers suggested that the threading process would be energetically unfavorable after studying the hydrolysis of flaps of varying lengths12. Furthermore, heavily modified 5′ flaps seemingly too big to transit such a small hole are nonetheless cleaved by the enzyme,13–15 casting doubt on the threading hypothesis and leading to alternative clamping or tracking models not involving a threading step12,13,16. On the other hand, subsequent biochemical studies suggested that threading may occur through a hole bounded by an initially disordered region of the enzyme17. Thus, the threading model has proved controversial. Although structures of FENs with bound cleavage products have been reported18,19, until now, no structures of intact DNA substrates threading through a FEN enzyme have been published.

We set out to produce mutant bacteriophage T5 flap endonuclease (T5Fen) proteins that retained DNA-binding, but not catalytic, activity in order to obtain structural information on the enzyme–substrate complex. Here we present crystal structures and biochemical analysis that elucidate the FEN mechanism. We show that substrate-free protein exists in conformations with a small or large hole. One complex with DNA shows single-stranded substrate poised to enter the enzyme. A second complex shows unequivocally that intact single-stranded DNA threads through the enzyme. These structures, and an additional pseudo-enzyme-product complex, provide unprecedented insight into the mechanism of these essential metalloenzymes.




Europe PMC Funders Author Manuscripts

## Results

Capturing the structure of an intact substrate-FEN complex faces an inherent challenge. The seven conserved acidic residues in the enzyme's active site bind magnesium ions required for catalysis. In the absence of these cations, the negatively-charged aspartate residues repel the DNA phosphodiester backbone hindering complex formation20. We reasoned that substituting an active-site aspartic acid residue such as Asp153 or Asp155 in the T5Fen with lysine might allow its positively charged ε-amino group to mimic one of the catalytically essential metal ions. Our aim was to produce a protein capable of binding, but not cutting DNA and thus suitable for co-crystallization with intact substrates. We first determined crystal structures of T5Fen and its D153K variant.

### Lysine's ε-amino group mimics a metal ion in T5FenD153K

In the absence of DNA T5Fen and T5FenD153K crystalized with $Mg^{2+}$ in essentially identical forms. Each diffracted to ~1.5 Å. In both cases, the crystals contained molecules in two different conformations in their asymmetric units (AU) (Fig. 1 a–d, Table 1 and Supplementary Fig. 1a–d). All had a globular domain housing two metal-binding regions designated as Cat1 and Cat2 (Fig. 1e). In one of the equivalent conformations observed in both T5Fen and the D153K variant, residues 84–92 were present as a helix (h4, Fig. 1a,c). However, these residues adopted a looped-out conformation in the second molecule in each AU (Fig. 1b,d). Both conformations contained a hole or channel situated above the active site. This hole was more than twice as large in the looped-out conformation than in the helical arch form (Fig. 1c,d). In wild type (wt) T5Fen, two $Mg^{2+}$ ions (M1 and M2) separated by 3.6 Å were bound through conserved residues in the Cat1 site of the helical arch form, (Fig. 1e). A third magnesium ion (M3) was bound in Cat2. The M1 and M3 sites were occupied by $Mg^{2+}$ ions in the molecule with the looped-out conformation (Fig. 1d,e).

The structures of the helical-arch and looped-out conformations of T5FenD153K with $Mg^{2+}$ were very similar to those in WT T5Fen. However, no metal ions were observed in Cat1 of either conformation in the D153K variant (Fig. 1f). Instead, the $\varepsilon$-amino group of Lys153 occupied the analogous position to M1 in the wt (Fig. 1f,g). It interacted electrostatically with conserved aspartic acids in Cat1. A water molecule occupied the M2 site rather than a cation. The T5FenD153K Cat2 residues bound a single $Mg^{2+}$ ion (Fig. 1f). Otherwise the conformations were isostructural with the wt protein. Thus, introduction of Lys153 did not perturb the overall architecture of the molecule (Supplementary Fig. 1a–c, and Supplementary Video 1).

We next assessed the impact of substituting aspartic acid with lysine on substrate recognition and binding. Single-stranded oligonucleotide ($dT_{12}$) was digested by wt T5Fen producing products of 3–5 nucleotides as expected21, whereas neither variant T5FenD153K nor a second variant, D155K, showed activity (Fig. 2a,b). Structure-specific nuclease activity was readily detected using a dual labelled substrate (Supplementary Fig. 2a) in T5Fen, but not in the variants (Fig. 2c). However, they were capable of binding DNA despite their negligible hydrolytic activity, interacting with a DNA flap more tightly than did wt protein as indicated by their reduced dissociation constants (Supplementary Fig. 2b,c).

### A pre-threading T5Fen–DNA complex

An eight base-pair duplex DNA possessing four single-stranded adenosines at each 5′ end was co-crystalized with the D153K variant and magnesium ions (Supplementary Fig. 3a). The crystals diffracted to 2.2 Å resolution (Table 1). The AU contained a protein molecule bound at each end of the DNA duplex (Supplementary Fig. 3b–d). The helical arch was intact in both molecules in the AU. The DNA did not contact the protein molecules in a symmetrical manner, but revealed two distinct types of interaction (complexes C1 and C2). In complex C1, the 5′ single-stranded end was positioned just below the arch, poised to enter it in a pre-threading binding mode (Fig. 3a,b and Supplementary Fig. 3b–d). The 5′ nucleotide of one strand engaged with residues on helices 1 and 4 placing it just in front of the hole beneath helices 4 and 5. Phe32 and His36 on helix 1 made Van der Waals (VdW) contact with the sugar and base of dA1 respectively (Fig. 3b) while its 3′ phosphate formed a salt bridge to Arg86 situated on helix 4. Water-mediated and direct hydrogen bonds between the dA3 phosphate group and the backbone amides of Asp155 and Gly154 helped to anchor the ssDNA in place. The ε-amino group of Lys153, introduced to mimic M1 in the Cat1 site, made a salt bridge with the dA2 phosphate (Fig. 3b). The dsDNA region contacted the helix-three-turn-helix motif (H3TH, Asp188–Gly225) (Fig. 3a,c). A potassium ion was bound via backbone carbonyl oxygens within this motif. It directly co-ordinated a phosphate group on the DNA duplex while an adjacent phosphodiester formed hydrogen bonds with backbone amides of conserved residues Lys215 and Arg216 (Fig. 3c). Further details are given in Supplementary Table 1.

### A fully-threaded DNA–T5Fen complex

In the second complex (C2), all four single-stranded nucleotides of the substrate threaded through the helical arch of T5FenD153K, bringing the phosphodiester backbone into intimate contact with the active site (Fig. 4a). The last base pair of the duplex (dG5:dC12) interacted with an intact helical-arch *via* residues Arg86 and Tyr90, and also with residues on h1 where dG5 made contact with Phe32 and was also hydrogen-bonded to Lys35 (Fig. 4b). An unexpected barb-like structure was adopted by the translocated single-stranded DNA (Fig. 4c–e). The purine rings of nucleotides 1, 3 and 4 formed a spiral stack but nucleotide 2 was flipped out by approximately 180° so that its base contacted Gly70, Lys71, Leu76, and Pro80 on the distal side of the hole (Fig. 4c). The DNA backbone traced out a path resembling the letter L as it passed from the H3TH motif over the Cat1 site and through the archway (Fig. 4d,e). The distortion of the backbone was partly due to strong electrostatic interactions between the phosphodiesters of nucleotides 3–5 as they wrapped around the positively charged guanidinium group of Arg86 on helix 4. Several other residues lining the helical arch contributed to distorting the DNA backbone including Asp87, Tyr90, Arg93, and Phe105.

A single $Mg^{2+}$ ion occupied the Cat1 M1 site while the metal-mimicking Lys153's ε-amino group was located 4 Å away at the M2 site. The scissile phosphodiester on the 3′ side of dG5 liganded the Cat1 M1 $Mg^{2+}$ ion (Fig. 4b,e). A $Mg^{2+}$ ion bound via conserved aspartic acid residues that make up the Cat2 metal-binding site provided further electrostatic interactions with the phosphate of dG7 (Fig. 4e). The duplex region of the substrate made

additional interactions (Supplementary Table 2) with the protein similar to those in the C1 complex.

## Structure of a pseudo-cleavage product-T5Fen complex

We obtained a complex (C3) with a second variant T5Fen (D155K) and a 17-residue oligonucleotide. Each protein molecule contacted different parts of three oligonucleotides in the crystal array (chains X, Y, Z, Fig. 5a and Supplementary Fig. 4a–c). The 5′ end of strand X follows the same path as the intact threaded strand in complex C2, passing over the H3TH motif and Cat1 site. The 3′ end of strand Z is stacked onto the 5′ end of strand X and continues under the helical arch. Hence, the resulting structure resembled a cleaved branched substrate lacking only the scissile phosphate (Supplementary Fig. 4b). It crystallized in the presence of calcium ions and diffracted to ~1.9 Å (Table 1). Calcium ions promote binding but not catalysis in T5Fen20. One strand (X) was straddled by the helical arch with its 3′ hydroxyl group (dG17) making polar contacts *via* Asn29 and an inner-sphere water molecule bound to $Ca^{2+}$ in the M1 site of Cat1 (Fig. 5a–d). The M2 site was occupied by the ε-amino group of Lys155 (Supplementary Fig. 4d). It made electrostatic interactions with conserved residues in Cat1 and Cat2. It also co-ordinated a water molecule that was hydrogen bonded to $Ca^{2+}$, just as a water molecule bridged the magnesium ions in the DNA-free T5Fen structure (Fig. 5d and Supplementary Fig. 4d). The base of dG17 of chain X stacked with the recessed 5′ end of chain Y and made a base pair with a nucleotide on chain Z (Fig. 5). The threaded nucleotides made further interactions with the protein (Fig. 5b–d). These include flipping of a nucleobase such that rather than being stacked between adjacent bases, it was rotated ~180° locating it adjacent to helix 3 on the distal side of the helical arch (Fig. 5b,c) similar to the barbed conformation observed in the C2 substrate complex. Residues within the H3TH domain hosted a potassium ion that formed polar contacts with the phosphodiester backbone (Supplementary Fig. 4e).

The C3 structure also provided additional insight into interactions of the substrate's 3′ single-stranded region with the protein (strand Y, Fig. 5). Conserved residue Arg33 on h1 contacted this region *via* a salt bridge (Supplementary Fig. 4f) explaining the results of previous mutagenesis studies in which an R33A variant binds DNA with lower affinity than wt22. Full details of the C3 complex's molecular interactions are given in Supplementary Table 3.

## Structural changes upon substrate binding

Comparison of the DNA-free, looped-out structure with threaded substrate complex revealed changes upon substrate binding (Supplementary Fig. 5a). Perhaps the most striking involved conserved amino acid Arg86. In the pre-threading complex, Arg86 was located in a very similar position to that seen in the DNA-free helical arch form (Supplementary Fig. 5b,c). Its side chain formed an angle of approximately 45° with the plane of helices 4 and 5, juxtaposing the charged guanidinium group with the H3TH domain in the vicinity of Cat2. Compared to the DNA-free structure in which residues 84–92 were looped out, the Arg86 guanidinium group was displaced by ~13 Å and its Cα atom by ~ 6 Å (Supplementary Fig. 5c). Helix 1 residues involved in substrate binding underwent movements of up to 7 Å to engage with DNA (Supplementary Fig. 5d). Lys215 and Arg216 in the H3TH motif were

displaced by ~ 3 and 6 Å respectively, upon DNA binding (Supplementary Fig. 5e), explaining previous results of mutagenesis studies on these conserved residues22.

### Metal ion binding in T5Fen

A two-metal-ion mechanism for FEN catalysis has been suggested23 similar to that proposed for the Klenow proofreading 3′–5′ exonuclease24. However, the metal ion separation observed in DNA-free FEN structures (5–8 Å) is generally too large for this mechanism, which requires spacings of 3–4 Å, casting doubt on its validity11,23,25. Our wt T5Fen structure revealed a pair of closely-spaced metals bound in Cat1 consistent with a two-metal-ion mechanism, as was the placement of these ions relative to the scissile phosphodiester (Fig. 1e and Supplementary Fig. 4d). The Cat2 metal binding site is completely conserved in FEN domains of prokaryotic DNA polymerase I but is absent in FENs from higher organisms and some bacterial homologs6,26. Cat2 is not essential for flap cleavage but is suggested to facilitate substrate binding18,20,26,27, as is the potassium ion bound to the H3TH motif. Our structures provide molecular details of these metal-substrate interactions (Figs. 3c,e, 4b,e and 5d, and Supplementary Fig. 4d,e).

### Structural conservation throughout the FEN-family

T5Fen shared low primary sequence identity with characterized homologues from bacteria and eukaryotes. Despite this the structural similarities are striking, suggesting common biochemistry (Fig. 6). The *E. coli* Exo IX FEN homolog, crystallized as a product complex with DNA18, shared ~25% amino acid identity with T5Fen yet they have 237 equivalent residues with a root-mean-square deviation (rmsd) of aligned Cαatoms of 2.4 Å (Fig. 6a). The active sites of these enzymes were similarly arranged with two closely-spaced divalent cations (Fig. 6b,c). Perhaps more surprising was the structural similarity that T5Fen shares with human FEN1 (rmsd of ~ 4.7 Å over 200 Cα atoms Fig. 6a–c). This was not limited to the overall topology but also extended to the active site and H3TH motif present in T5, *E. coli* and human FEN homologs (Supplementary Fig. 4e). Thus, FENs are structurally conserved in diverse organisms. The H3TH motif hosts a potassium ion that mediates electrostatic interactions with DNA in all three enzymes18,19.

## Discussion

The FEN family includes structure-specific nucleases capable of cleaving flaps, nicks and gapped structures. How FEN enzymes cleave bifurcated DNA to generate sealable nicks has been the subject of debate since Lyamichev and co-workers proposed that the single-stranded 5′-flap branch might thread through a FEN protein10. Hydrolysis would occur once the enzyme reached the junction with double-stranded DNA where it would halt due to the size restriction imposed by its hole. However, it was suggested that such a threading mechanism would be thermodynamically unfavorable12. Recent structural studies have added to the controversy. A study involving FEN homolog ExoI led the authors to propose a mechanism lacking a threading step28 while structural studies on human FEN1, complexed with cleaved products (not intact substrates) and heavy-metal ions, support a threading hypothesis but did not provide structures showing threading19,28. Facilitated by our metal-




Europe PMC Funders Author Manuscripts

mimic mutagenesis approach, a unique series of molecular snapshots characterizing the entire FEN reaction pathway has emerged.

## A fly-casting, thread, bend, and barb mechanism

The seemingly unlikely event of threading ssDNA through a small hole in a protein may be facilitated by first binding the flap's dsDNA region to the FEN in a bind-then-thread mechanism12. Once bound, the increased local concentration of the 5′ end of the substrate in the vicinity of any hole in the enzyme would increase the likelihood of their interaction. Building on this, it was proposed previously that a disordered "arch", with a hole larger than previously characterized by X-ray crystallography, could facilitate passage of ssDNA and further reduce theoretical objections based on thermodynamic grounds17. A disordered-to-ordered transition follows the threading step. The alternative conformations of residues 84–92 in the looped-out and helical-arch forms in our T5Fen provided structural evidence for this mechanism (Fig. 1b,d). The approximate dimensions of the ovoid channel through the looped-out form being 12 × 17 Å compared with 8 × 11 Å in the helical-arch conformation. Furthermore, the helical arch is entirely disordered in the crystal structure of T5Fen variant K83A, demonstrating flexibility of this region29. Similarly, the equivalent region in other published FEN structures is disordered23,25. We speculate that the enzyme uses a "fly-casting mechanism" of molecular recognition as proposed for transcription factor binding site interactions in which disordered receptors capture their ligands more efficiently than when ordered, resulting in enhanced binding kinetics30.

In our threaded substrate complex, deoxyadenosines 1, 3, and 4 formed a spiral base-stack on exiting the helical arch. Whereas, dA2 was flipped 180° so the base contacting helix 3 was four nucleotides from the scissile bond and thus formed a structure resembling a barb. Similarly the barb-like conformation seen in the pseudo-product complex was located five nucleotides from the cleavage site. These findings provided a physical rationale for the observation that exonucleolytic FEN products range from 3–5 nucleotides in length20,21. The nucleotide "barb", once engaged with the hydrophobic patch, could lock down the substrate in optimal contact with the active site thus promoting catalysis (Supplementary Video 2). This was facilitated by Arg86 in the intact substrate complex (C2). Compared with its position in free protein, it pivoted towards helix 3 and away from the Cat1/Cat2 sites thereby bending the DNA into an "L" shape through contacts with 3 adjacent phosphodiesters. The importance of the equivalent arginine residue in a range of FENs from phage to man has been noted31,32. In the pseudo-enzyme-product complex Arg86 had swung back towards Cat1, contacting the newly revealed 5′ terminus. In a real catalytic event this terminus would have a phosphate group carrying two negative charges. The threaded product would dissociate from the enzyme allowing the new 5′ end to enter the arch for the next catalytic cycle fueled by energy of nucleotide hydrolysis and Brownian motion33.

We generated a model of the molecular transitions that may occur during catalysis based on superpositions of the structures of our DNA-free, fully-threaded and pseudo-product T5Fen complexes (Fig. 7a).

Once threaded and ordered, the substrate is bound such that one of the scissile phosphates acts as an inner sphere ligand for M1 in Cat1 (Fig. 7b). A water molecule that bridges the two Cat1 $Mg^{2+}$ ions is poised to attack the DNA backbone at a distance of ~2.6 Å from the scissile phosphate. This is similar to the two-metal-ion-mechanism proposed for Klenow proofreading exonuclease24. A ~1.3 Å movement would place this potential nucleophile appropriately to initiate formation of the transition state (TS). Thus, the nucleophile and 3′-hydroxyl leaving group would form the apical ligands of the trigonal-bipyramidal TS intermediate (Fig. 7c). As the new O-P bond forms, the 3′-O bond lengthens concomitantly leading to collapse of the TS. The attacking oxygen now ligands both M1 and M2 as part of the 5′-phosphate product (Fig. 7d).

Apart from their crucial roles in DNA replication and repair, FEN homologs such as Taq polymerase are also central to real-time quantitative PCR and clinical diagnostics34, and have also been proposed as potential therapeutic targets35. Better understanding of their biology could impact on these areas. We have shown a series of snapshots in the FEN-catalyzed hydrolysis reaction from free enzyme to pseudo-product complex via pre-threading and fully threaded intermediates. They revealed that DNA can indeed pass through the channel present in a FEN family member. Our results represent a distinct improvement in our understanding of the processing of branched DNA substrates, a process common to all life, and highlight the likely conservation of mechanism across the phyla.

## Methods

### Data reporting

No statistical methods were used to predetermine sample size. The investigators were not blinded to allocation during experiments and outcome assessment.

Original images of gels, autoradiographs and blots used in this study can be found in Supplementary Data Set 1.

### Site directed mutagenesis

Site-directed mutagenesis of the T5Fen (also known as the gene D15 product, accession number NC_005859.1, nucleotides 80,134–80,968), was conducted using oligonucleotides: D153K (dATCGTCTGCTTCTACACCACAAATGGTAAAAGTTGG) and D155K (dGTTAATAAAGTATCCCATTTACCATCTGTAGATATTAG) supplied by EurofinsMWG using the method previously described36. Both wild type and mutant T5Fen encoding sequences were cloned into the heat inducible pJONEX vector.

### Protein production and purification

Expression of T5Fen proteins was carried out as described previously21 using the appropriate pJONEX4 derivative in *E. coli* strain M72(λ)37. Briefly, cells were grown to mid-log phase in 5 L of rich media containing 100 μg/ml of carbenicillin at 28°C. Protein expression was induced by increasing the temperature to 42°C for 3 hours. Purification of proteins for biochemical assays was carried out as described previously20–22, 38. Proteins for crystallization were purified by modification of these procedures and included addition

of a size exclusion chromatography step. Briefly, initial purification was performed using a Heparin-HP chromatography column at pH 8.0 followed by anion exchange chromatography on a Resource Q column at pH 6.5. Protein was applied to a 1.6 × 60 cm Superdex-200 (GEHealthcare) size exclusion chromatography equilibrated with 20 mM HEPES pH 7.0, 150 mM KCl, 0.1 mM EDTA, 1 mM DTT at a flow rate of 1 ml/min. Fractions were collected and the protein concentration for each determined using the BioRad protein assay39. Proteins were concentrated using centrifugal diafiltration (Viva Spin units, vivaScience) to ~ 15 mg/ml. Sample purity was examined by SDS PAGE.

### Real-time structure-specific endonuclease assays

Structure-specific endonuclease activity was monitored in a continuous FRET-based assay adapted from the literature40. Oligonucleotide substrate OHP2 (5'-Cy3-CTCTGTCGAACACACGCXTGCGTGTGTTC, supplied by EurofinsMWG) labeled at a dU derivative (X) with FAM was used as the substrate (Supplementary Fig. 2a). Oligo OHP_2 was dissolved to a final concentration of 0.1 mM in TE buffer at pH 7. Exonuclease activity was also monitored using dual-labeled poly dT oligonucleotide FAM_BHQ_T12 (5′-FAM-TTTTTTTTTTTTBHQ). Initial rates of reactions were determined at substrate concentrations ranging from 6.25 nM to 250 nM in a buffer containing 25 mM of HEPES-NaOH pH 7, 100 mM of KCl, 10 mM $MgCl_2$, 2 mM DTT and 0.1 mg/ml BSA and the increase in fluorescence was monitored over time. The catalytic parameters of wild type T5Fen were determined and compared using nonlinear regression of the Michaelis-Menten equation and data were presented using Hanes-Woolf plot while the initial velocity of the reaction is determined by the linear region of the progress curve during the first few percent towards total completion of the reaction. The fluorescent emission intensity data were collected on a HITACHI F-2500 FL Spectrophotometer at 496 nm/519 nm (excitation/emission wavelengths) at 1 second intervals. Mean and range of the three repeats plotted (Fig. 2c) compared with negative control (–ve) with no added enzyme.

### Binding Studies

Aliquots of 199 μl of buffer containing 1 nM substrate were mixed with 1 μl of protein at different concentrations and incubated at room temperature for 20 minutes. The 200 μl sample was transferred into a 4-window quartz cuvette and placed in HITACHI F-2500 FL Spectrophotometer with polarizer mounted. Samples were excited with polarized light at 496 nm and readings of fluorescence emission were taken at 519 nm in both vertical and horizontal positions. The light intensities ($I$) were defined as following: $I_{VV}$ is for both excitation and emission polarizer mounted vertically, $I_{HH}$ is for both excitation and emission polarizer mounted horizontally, $I_{VH}$ uses the excitation polarizer vertical and emission polarizer horizontal, $I_{HV}$ uses the excitation polarizer horizontal and emission polarizer vertical. Anisotropy ($A$) is defined as $A = (I_{VV} - GI_{VH})/(I_{VV} + 2GI_{VH})$ where G-factor (G) is equal to $I_{VH}/I_{HH}$ (ref. 41). Experiments were repeated 3 times.

### Crystallization and structure determination of T5Fen and T5FenD153K proteins

T5Fen and its variants were used at a concentration of 15 mg/ml for both protein and protein-DNA complex crystallizations. Extensive screening of crystallization conditions was performed by the vapor diffusion technique at 7° and 17°C. Subsequently, good quality

diffraction data were collected at the Diamond Light Source, UK (X-ray beamline IO3) from crystals grown in conditions optimized from those found in the screens. Crystallization of the wt T5Fen and its D153K variant incorporated 200 mM $MgCl_2$ with the protein solution. For the wt T5Fen, the best diffraction was obtained from a crystal grown at 7°C in 0.2 M NaBr, 0.1 M Bis-Tris propane buffer pH 8.0, 22% $^{w}/_{v}$ PEG 3350. The T5FenD153K variant also crystallized at 7°C with the optimum conditions being 0.2 M NaI, 0.1 M Bis-Tris propane buffer pH 7.5, 23-25% $^{w}/_{v}$ PEG 3350. Crystals were cryoprotected by transfer into a solution matching the growth condition plus 20% $^{w}/_{v}$ ethylene glycol. Data collection statistics are summarized in Table 1.

## Co-crystallization with DNA substrates

Two separate self-annealing oligonucleotides were used. Oligonucleotides 5ov4 (5′-dAAAAGCGTACGC-3′), which gave an 8 base pair region plus a 4 nucleotide overhang at each 5’ end when self-annealed and 3ov6 (5′-dGATCTATATGCCATCGG-3′), which produces a 10 base pair region with two mismatches and a “flipped out” nucleotide plus 6 nucleotide overhang at each 3′ end after annealing and mixing with the protein (Supplementary Fig. 4). The concentration of both oligonucleotides was adjusted to 1.1 mM for the duplex molecule by dissolving each one in 10 mM MES pH 6.5 and 50 mM KCl. They were annealed by heating to 94°C for 10 minutes and allowed to cool to room temperature. Crystals with oligonucleotide 5ov4 were grown at 17°C with the D153K variant of T5Fen. The resulting T5FenD153K–5ov4 structure was determined from crystals grown in 0.2 M $MgCl_2$, 0.1 M Bis-Tris buffer pH 5.5, 25% $^{w}/_{v}$ PEG 3350. Crystals of the T5FenD155K with oligonucleotide 3ov6 grew in 0.2 M $CaCl_2$, 0.1 M sodium acetate buffer pH 5, 20% $^{w}/_{v}$ PEG 6000. In all cases, the protein-DNA complex crystals were cryoprotected by transfer into a solution matching the growth condition plus 30% $^{v}/_{v}$ glycerol. The processing of X-ray diffraction data for all crystals with or without DNA was performed using the in-house xia242 or iMosflm software43 at the Diamond Light Source (UK) using beamlines I-24 (T5FenD153K–5ov4) and I02 (T5FenD155K–3ov6), followed by scaling with XDS/XSCALE44 or SCALA45. Data collection and refinement statistics are summarized in Table 1.

## Structure determination and refinement

The structures of wt T5Fen and the D153K variant without DNA were determined by molecular replacement using the program PHASER46 with the previously determined 2.8 Å structure of the enzyme in complex with $Mn^{2+}$ (PDB entry 1UT5) as a search model20. In both cases, two molecules were found in the asymmetric unit and subsequent rounds of fitting and refinement were carried using COOT47 and REFMAC548. Structures were validated within COOT and by use of MOLPROBITY49. The structure of T5FenD153K–5ov4 complex was solved by molecular replacement using PHASER with T5Fen structure (PDB entry 1EXN) as the search model11. The D153K model determined in this study was used in molecular replacement as the search model for the T5FenD155K–3ov6 structure. Subsequent model building and refinement followed the same pattern as above for the protein alone utilizing the COOT, REFMAC and MOLPROBITY programs. Identification of metal cations and solvent anions in all structures was carried out on the basis of an analysis

of coordination geometry, ion environment, bond lengths and refined B-factors and CheckMyMetal web server50.

Ramachandran analysis of backbone torsion angles revealed no outliers for either the T5Fen (99% favored, remainder allowed conformations) or D153K variant models (>99% favored, remainder allowed conformations). Similarly, no outliers for either the T5FenD153K–5ov4 (99% favored, 1% in allowed conformations) or T5FenD155K–3ov6 (99% favored, 1% in allowed conformations) were observed. Data collection and refinement statistics are summarized in Table 1

## Supplementary Material

Refer to Web version on PubMed Central for supplementary material.

## Acknowledgments

F.A.A. was supported by a scholarship from Taif University. M.F. and C.S.F. were supported by scholarships from the University of Sheffield. Infrastructure was supported through Biotechnology and Biological Research Council (UK) grant awards 50/B19466 (J.R.S.) and REI18458 (J.R.S.).

## References

1. Burgers PM. Polymerase dynamics at the eukaryotic DNA replication fork. J Biol Chem. 2009; 284:4041–4045. [PubMed: 18835809]
2. Zechner EL, Wu CA, Marians KJ. Coordinated leading– and lagging–strand synthesis at the *Escherichia coli* DNA replication fork. III. A polymerase–primase interaction governs primer size. J Biol Chem. 1992; 267:4054–4063. [PubMed: 1531480]
3. Smith DJ, Whitehouse I. Intrinsic coupling of lagging–strand synthesis to chromatin assembly. Nature. 2012; 483:434–438. [PubMed: 22419157]
4. Maga G, et al. Okazaki fragment processing: modulation of the strand displacement activity of DNA polymerase delta by the concerted action of replication protein A, proliferating cell nuclear antigen, and flap endonuclease–1. Proc Natl Acad Sci USA. 2001; 98:14298–14303. [PubMed: 11724925]
5. Hobbs LJ, Nossal NG. Either bacteriophage T4 RNase H or *Escherichia coli* DNA polymerase I is essential for phage replication. J Bacteriol. 1996; 178:6772–857. [PubMed: 8955295]
6. Fukushima S, Itaya M, Kato H, Ogasawara N, Yoshikawa H. Reassessment of the *in vivo* functions of DNA polymerase I and RNase H in bacterial cell growth. J Bacteriol. 2007; 189:8575–83. [PubMed: 17905985]
7. Diaz A, Lacks SA, Lopez P. The 5' to 3' exonuclease activity of DNA polymerase I is essential for *Streptococcus pneumoniae*. Mol Microbiol. 1992; 6:3009–3019. [PubMed: 1336089]
8. Bayliss CD, Sweetman WA, Moxon ER. Destabilization of tetranucleotide repeats in *Haemophilus influenzae* mutants lacking RnaseHI or the Klenow domain of PolI. Nucleic Acids Res. 2005; 33:400–408. [PubMed: 15653640]
9. Kucherlapati M, et al. Haploinsufficiency of Flap endonuclease (Fen1) leads to rapid tumor progression. Proc Natl Acad Sci USA. 2002; 99:9924–9929. [PubMed: 12119409]
10. Lyamichev V, Brow MA, Dahlberg JE. Structure–specific endonucleolytic cleavage of nucleic acids by eubacterial DNA polymerases. Science. 1993; 260:778–783. [PubMed: 7683443]
11. Ceska TA, Sayers JR, Stier G, Suck D. A helical arch allowing single–stranded DNA to thread through T5 5'–exonuclease. Nature. 1996; 382:90–93. [PubMed: 8657312]
12. Xu Y, Potapova O, Leschziner AE, Grindley ND, Joyce CM. Contacts between the 5' nuclease of DNA polymerase I and its DNA substrate. J Biol Chem. 2001; 276:30167–30177. [PubMed: 11349126]

Europe PMC Funders Author Manuscripts


13. Bornarth CJ, Ranalli TA, Henricksen LA, Wahl AF, Bambara RA. Effect of flap modifications on human FEN1 cleavage. Biochemistry. 1999; 38:13347–13354. [PubMed: 10529210]
14. Zheng L, et al. Novel function of the flap endonuclease 1 complex in processing stalled DNA replication forks. EMBO Rep. 2005; 6:83–89. [PubMed: 15592449]
15. Liu R, Qiu J, Finger LD, Zheng L, Shen B. The DNA–protein interaction modes of FEN–1 with gap substrates and their implication in preventing duplication mutations. Nucleic Acids Res. 2006; 34:1772–1784. [PubMed: 16582103]
16. Gloor JW, Balakrishnan L, Bambara RA. Flap endonuclease 1 mechanism analysis indicates flap base binding prior to threading. J Biol Chem. 2010; 285:34922–34931. [PubMed: 20739288]
17. Patel N, et al. Flap endonucleases pass 5'–flaps through a flexible arch using a disorder–thread–order mechanism to confer specificity for free 5'–ends. Nucleic Acids Res. 2012; 40:4507–19. [PubMed: 22319208]
18. Anstey–Gilbert CS, et al. The structure of *Escherichia coli* ExoIX–implications for DNA binding and catalysis in flap endonucleases. Nucleic Acids Res. 2013; 41:8357–8367. [PubMed: 23821668]
19. Tsutakawa SE, et al. Human flap endonuclease structures, DNA double–base flipping, and a unified understanding of the FEN1 superfamily. Cell. 2011; 145:198–211. [PubMed: 21496641]
20. Feng M, et al. Roles of divalent metal ions in flap endonuclease–substrate interactions. Nat Struct Mol Biol. 2004; 11:450–456. [PubMed: 15077103]
21. Sayers JR, Eckstein F. Properties of overexpressed phage–T5 D15 exonuclease – Similarities with *Escherichia coli* DNA–polymerase–I 5'–3' exonuclease. J Biol Chem. 1990; 265:18311–18317. [PubMed: 2211703]
22. Dervan JJ, et al. Interactions of mutant and wild–type flap endonucleases with oligonucleotide substrates suggest an alternative model of DNA binding. Proc Natl Acad Sci USA. 2002; 99:8542–8547. [PubMed: 12084915]
23. Kim Y, et al. Crystal structure of *Thermus aquaticus* DNA polymerase. Nature. 1995; 376:612–616. [PubMed: 7637814]
24. Beese LS, Steitz TA. Structural basis for the 3'–5' exonuclease activity of *Escherichia coli* DNA polymerase I: a two metal ion mechanism. EMBO J. 1991; 10:25–33. [PubMed: 1989886]
25. Mueser TC, Nossal NG, Hyde CC. Structure of bacteriophage T4 RNase H, a 5' to 3' RNA–DNA and DNA–DNA exonuclease with sequence similarity to the RAD2 family of eukaryotic proteins. Cell. 1996; 85:1101–1112. [PubMed: 8674116]
26. Allen LM, Hodskinson MR, Sayers JR. Active site substitutions delineate distinct classes of eubacterial flap endonuclease. Biochem J. 2009; 418:285–292. [PubMed: 19000038]
27. Tomlinson CG, et al. Neutralizing mutations of carboxylates that bind metal 2 in T5 flap endonuclease result in an enzyme that still requires two metal ions. J Biol Chem. 2011; 286:30878–30887. [PubMed: 21734257]
28. Orans J, et al. Structures of human exonuclease 1 DNA complexes suggest a unified mechanism for nuclease family. Cell. 2011; 145:212–223. [PubMed: 21496642]
29. Garforth SJ, Ceska TA, Suck D, Sayers JR. Mutagenesis of conserved lysine residues in bacteriophage T5 5'–3' exonuclease suggests separate mechanisms of endo–and exonucleolytic cleavage. Proc Natl Acad Sci USA. 1999; 96:38–43. [PubMed: 9874768]
30. Shoemaker BA, Portman JJ, Wolynes PG. Speeding molecular recognition by using the folding funnel: the fly–casting mechanism. Proc Natl Acad Sci USA. 2000; 97:8868–8873. [PubMed: 10908673]
31. Bhagwat M, Hobbs LJ, Nossal NG. The 5'–exonuclease activity of bacteriophage T4 RNase H is stimulated by the T4 gene 32 single–stranded DNA–binding protein, but its flap endonuclease is inhibited. J Biol Chem. 1997; 272:28523–28530. [PubMed: 9353314]
32. Finger LD, et al. Observation of unpaired substrate DNA in the flap endonuclease–1 active site. Nucleic Acids Res. 2013; 41:9839–9847. [PubMed: 23975198]
33. Ptacin JL, et al. A spindle–like apparatus guides bacterial chromosome segregation. Nat Cell Biol. 2010; 12:791–798. [PubMed: 20657594]
34. Gibson UE, Heid CA, Williams PM. A novel method for real time quantitative RT–PCR. Genome Res. 1996; 6:995–1001. [PubMed: 8908519]

35. McWhirter C, et al. Development of a high–throughput fluorescence polarization DNA cleavage assay for the identification of FEN1 inhibitors. J Biomol Screen. 2013; 18:567–575. [PubMed: 23427045]
36. Sayers JR, Krekel C, Eckstein F. Rapid high–efficiency site–directed mutagenesis by the phosphorothioate approach. Biotechniques. 1992; 13:592–596. [PubMed: 1476729]
37. Sayers JR, Eckstein F. A single–strand specific endonuclease activity copurifies with overexpressed T5 D15 exonuclease. Nucleic Acids Res. 1991; 19:4127–4132. [PubMed: 1651477]
38. Garforth SJ, Sayers JR. Structure–specific DNA binding by bacteriophage T5 5–3' exonuclease. Nucleic Acids Res. 1997; 25:3801–3807. [PubMed: 9380501]
39. Bradford MM. A rapid and sensitive method for the quantitation of microgram quantities of protein utilizing the principle of protein–dye binding. Anal Biochem. 1976; 72:248–254. [PubMed: 942051]
40. Hutton RD, Craggs TD, White MF, Penedo JC. PCNA and XPF cooperate to distort DNA substrates. Nucleic Acids Res. 2010; 38:1664–1675. [PubMed: 20008103]
41. Heyduk T, Ma Y, Tang H, Ebright RH. Fluorescence anisotropy: rapid, quantitative assay for protein–DNA and protein–protein interaction. Methods Enzymol. 1996; 274:492–503. [PubMed: 8902827]
42. Winter G, Lobley CM, Prince SM. Decision making in xia2. Acta Crystallogr D Biol Crystallogr. 2013; 69:1260–1273. [PubMed: 23793152]
43. Battye TG, Kontogiannis L, Johnson O, Powell HR, Leslie AG. iMOSFLM: a new graphical interface for diffraction–image processing with MOSFLM. Acta Crystallogr D Biol Crystallogr. 2011; 67:271–281. [PubMed: 21460445]
44. Kabsch W. Integration, scaling, space–group assignment and post–refinement. Acta Crystallogr D Biol Crystallogr. 2010; 66:133–144. [PubMed: 20124693]
45. Evans P. Scaling and assessment of data quality. Acta Crystallogr D Biol Crystallogr. 2006; 62:72–82. [PubMed: 16369096]
46. McCoy AJ, et al. Phaser crystallographic software. J Appl Crystallogr. 2007; 40:658–674. [PubMed: 19461840]
47. Emsley P, Lohkamp B, Scott WG, Cowtan K. Features and development of Coot. Acta Crystallogr D Biol Crystallogr. 2010; 66:486–501. [PubMed: 20383002]
48. Murshudov GN, et al. REFMAC5 for the refinement of macromolecular crystal structures. Acta Crystallogr D Biol Crystallogr. 2011; 67:355–367. [PubMed: 21460454]
49. Chen VB, et al. MolProbity: all–atom structure validation for macromolecular crystallography. Acta Crystallogr D Biol Crystallogr. 2010; 66:12–21. [PubMed: 20057044]
50. Zheng H, et al. Validation of metal–binding sites in macromolecular structures with the CheckMyMetal web server. Nat Protoc. 2013; 9:156–170. [PubMed: 24356774]


Europe PMC Funders Author Manuscripts

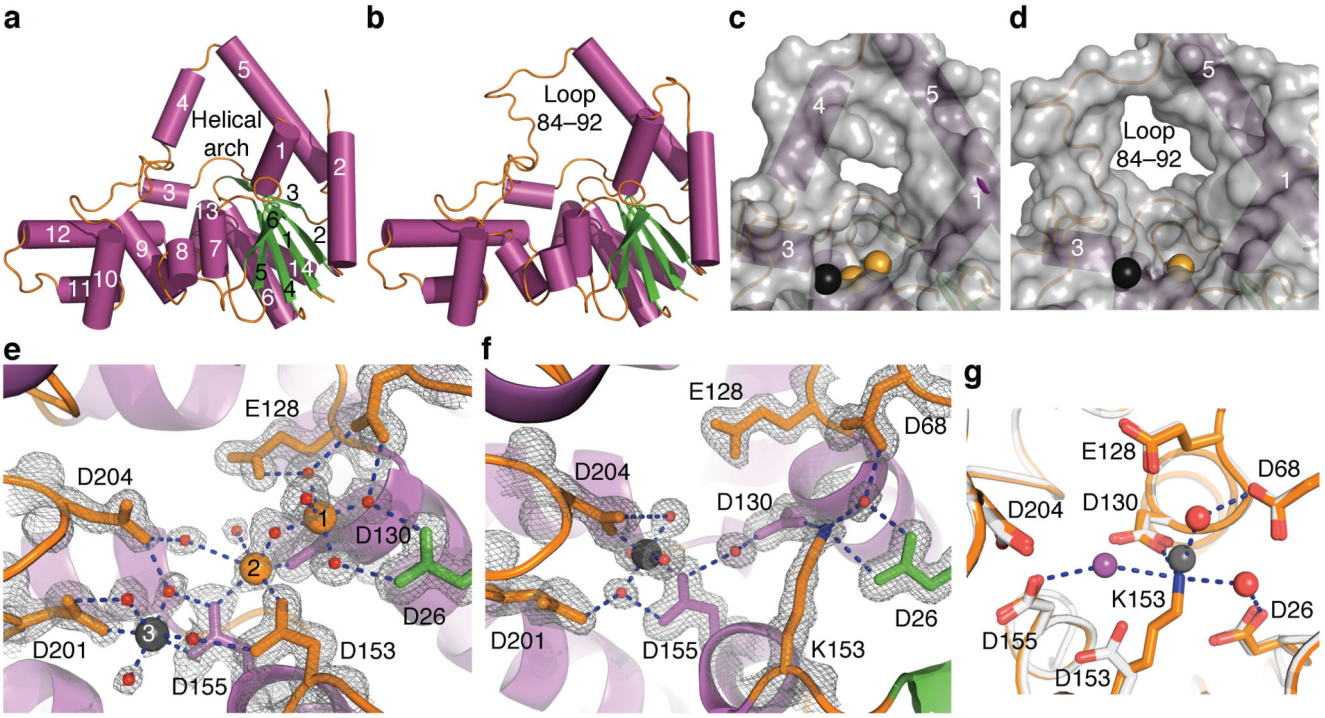


**Figure 1.**

T5Fen structures and activities. (**a,b**) Cartoon representation of T5Fen in helical arch (**a**) and looped conformations (**b**) with helices shown in magenta and β strands in green (numbered in white and black, respectively). (**c,d**) Close-up view of channel through T5Fen (orange spheres, Cat1 $Mg^{2+}$; black spheres, $Mg^{2+}$ Cat2). (**e,f**) Side chains of metal-liganding residues shown as sticks, colored according to secondary structure with electron density contoured at 1.2 sigma from a final 2Fo–Fc map (grey mesh) for T5Fen (**e**) and D153K variant with waters molecules shown as red spheres (**f**). (**g**) Cat1 sites of D153K and wt T5Fen superimposed (orange and grey backbones respectively) with grey sphere indicating position of magnesium M1 in (**e**), and water molecule at M2 site in D153K variant (magenta sphere).




Europe PMC Funders Author Manuscripts

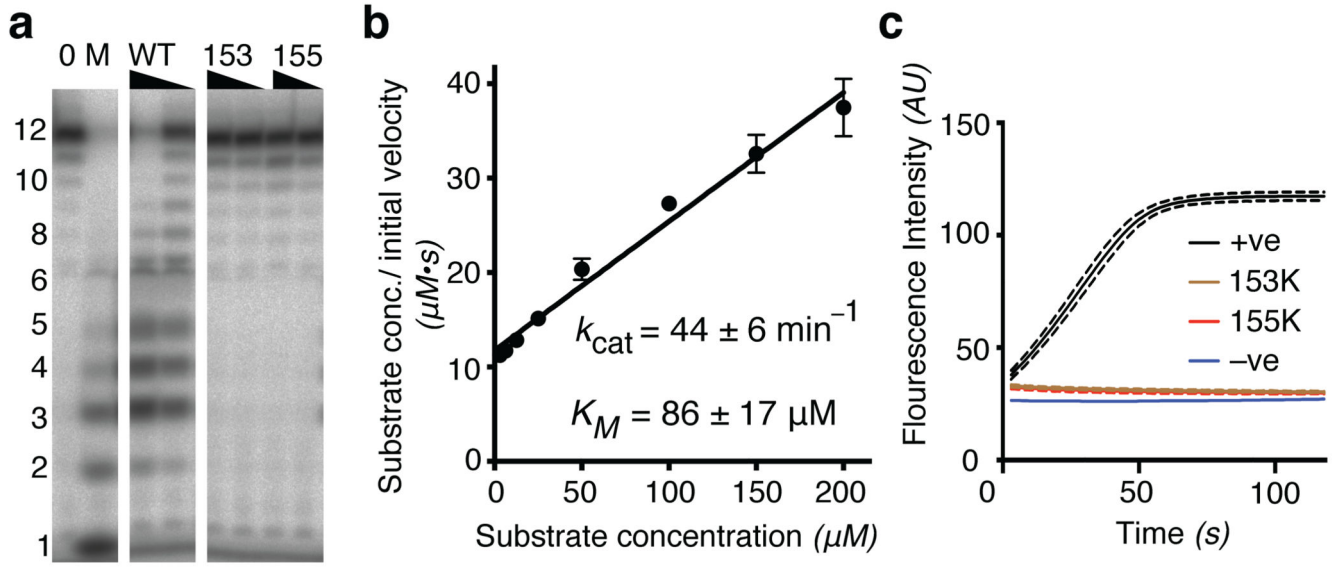


**Figure 2.**

T5Fen variants D153K and D155K lack enzymatic activity. (**a**) Radiolabelled dT12 (lane 0) reacted with wild type (WT), 153K or 155K variant T5Fen protein as indicated. Lane M, mononucleotide ladder. Original images of the gel can be found in *+. (**b**) Kinetics of WT T5Fen-catalyzed oligo-dT hydrolysis (error bars represent s.e.m. of 3 technical replicates). (**c**) Structure-specific endonuclease activity progress curves for WT (+ve), negative control (–ve) and variants indicated. Means (solid lines) and range (dashes) of 3 technical replicates indicated (AU, arbitrary units).





Europe PMC Funders Author Manuscripts

Europe PMC Funders Author Manuscripts

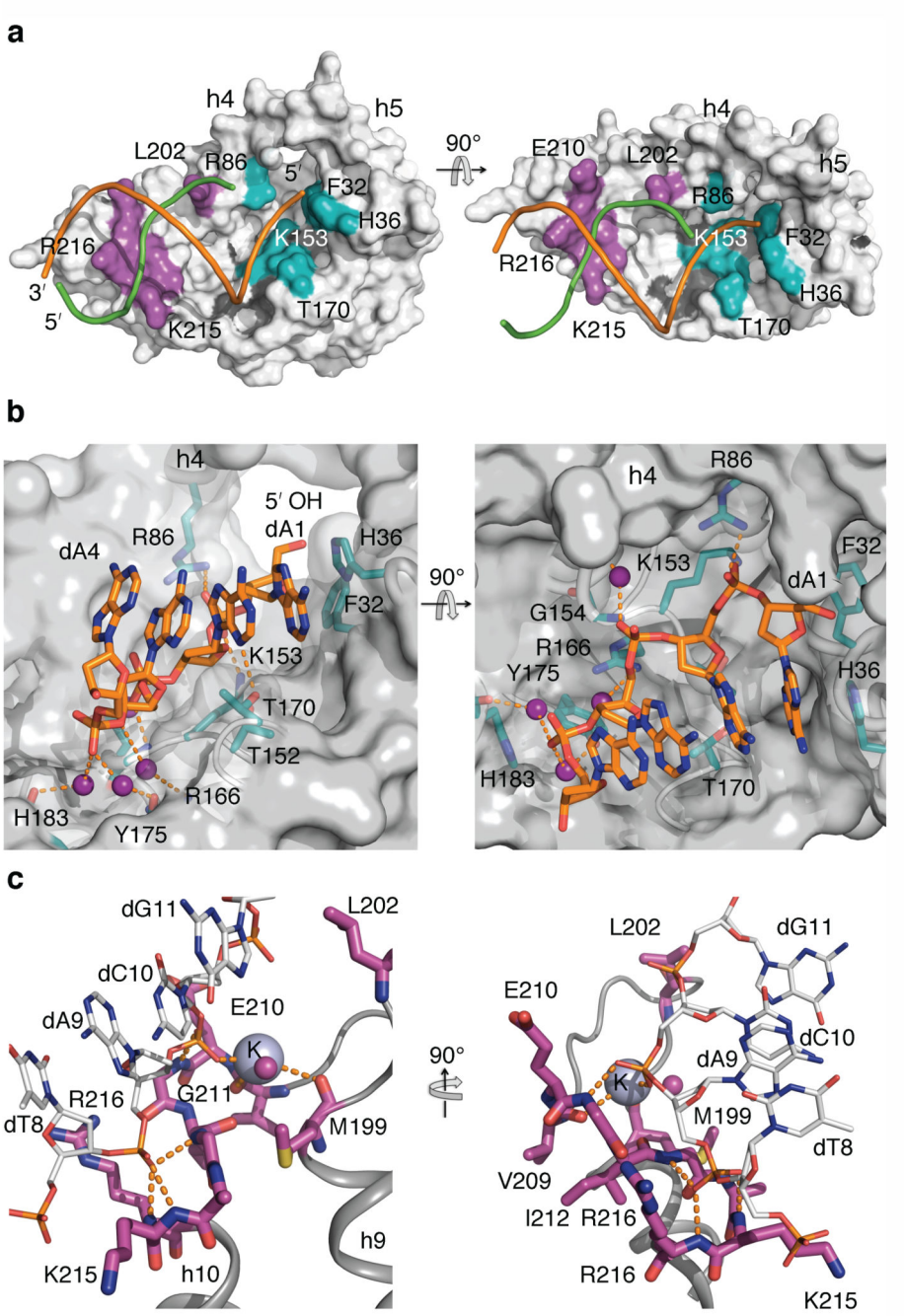


**Figure 3.**

Protein–DNA interactions in pre-threading T5Fen complex C1. (**a**) Residues within 4 Å of strand X (orange cartoon) or strand Y (green cartoon) colored cyan and magenta, respectively. Helices h4 and h5 indicated. (**b**) Hydrogen bonds and salt bridges between protein and DNA shown as(orange dashes). Residues within 4 Å shown as sticks. (**c**) Strand Y nucleotides 8–11 in duplex region (wireframe) contact residues (magenta sticks) in the H3TH motif either *via* VdW or hydrogen bonds (orange dashes).

Europe PMC Funders Author Manuscripts

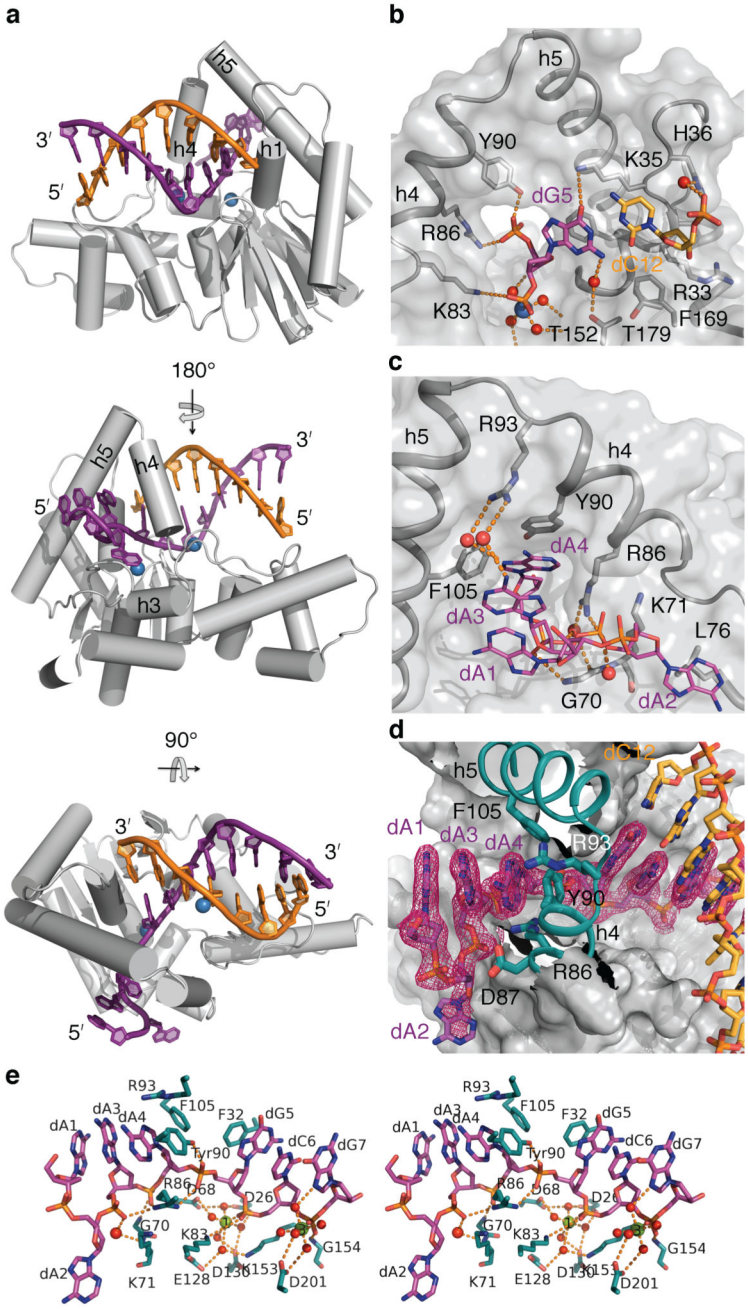


**Figure 4.**

Structure of a fully threaded DNA complex C2. (**a**) Three views of T5FenD153K in complex with $Mg^{2+}$ (blue spheres) and DNA. (**b**) Contacts to last base pair of duplex (5′dG5:3′dC1 magenta and yellow carbon sticks), showing amino acids within 4 Å (grey sticks). (**c**) Details of protein interactions with nucleotides dA1–4. (**d**) Electron density for DNA (magenta mesh, contoured at 1 sigma). Residues within 4 Å on the helical arch in cyan sticks. (**e**) Stereo diagram showing threaded DNA axis distorted through ~90°. $Mg^{2+}$ ions at

M1 and M3 as green spheres. Key residues involved in binding shown as sticks. Waters shown as red spheres, with hydrogen bonds and polar contacts as orange dashes.



Europe PMC Funders Author Manuscripts

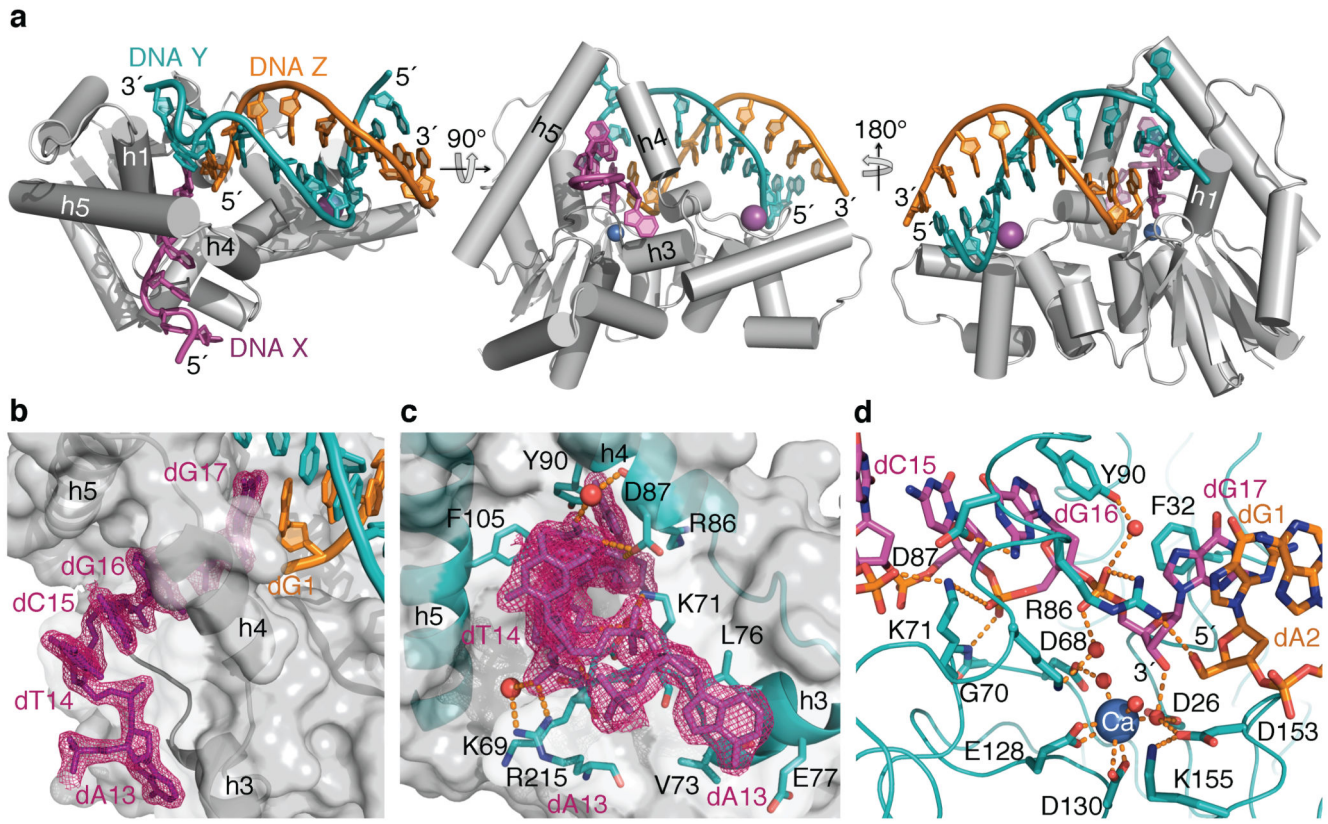


**Figure 5.**

Structure of pseudo-enzyme-product complex. (**a**) Three views of complex. Calcium and potassium ions as blue and magenta spheres, respectively. (**b**) Electron density contoured at 1.5 sigma for DNA-X (magenta mesh). (**c**) View corresponding to center panel above. Residues within VdW contact of DNA-X shown as sticks with cyan carbon atoms. Polar contacts (orange dashes) between substrate and bound solvent (red spheres). (**d**) Detail of active site showing polar contacts around the 3′-end of strand X (magenta) and the 5′-hydroxyl of strand Z (orange). Arg86 contacted strands X and Z. Lys155 occupied the Cat1 M2 site.




Europe PMC Funders Author Manuscripts

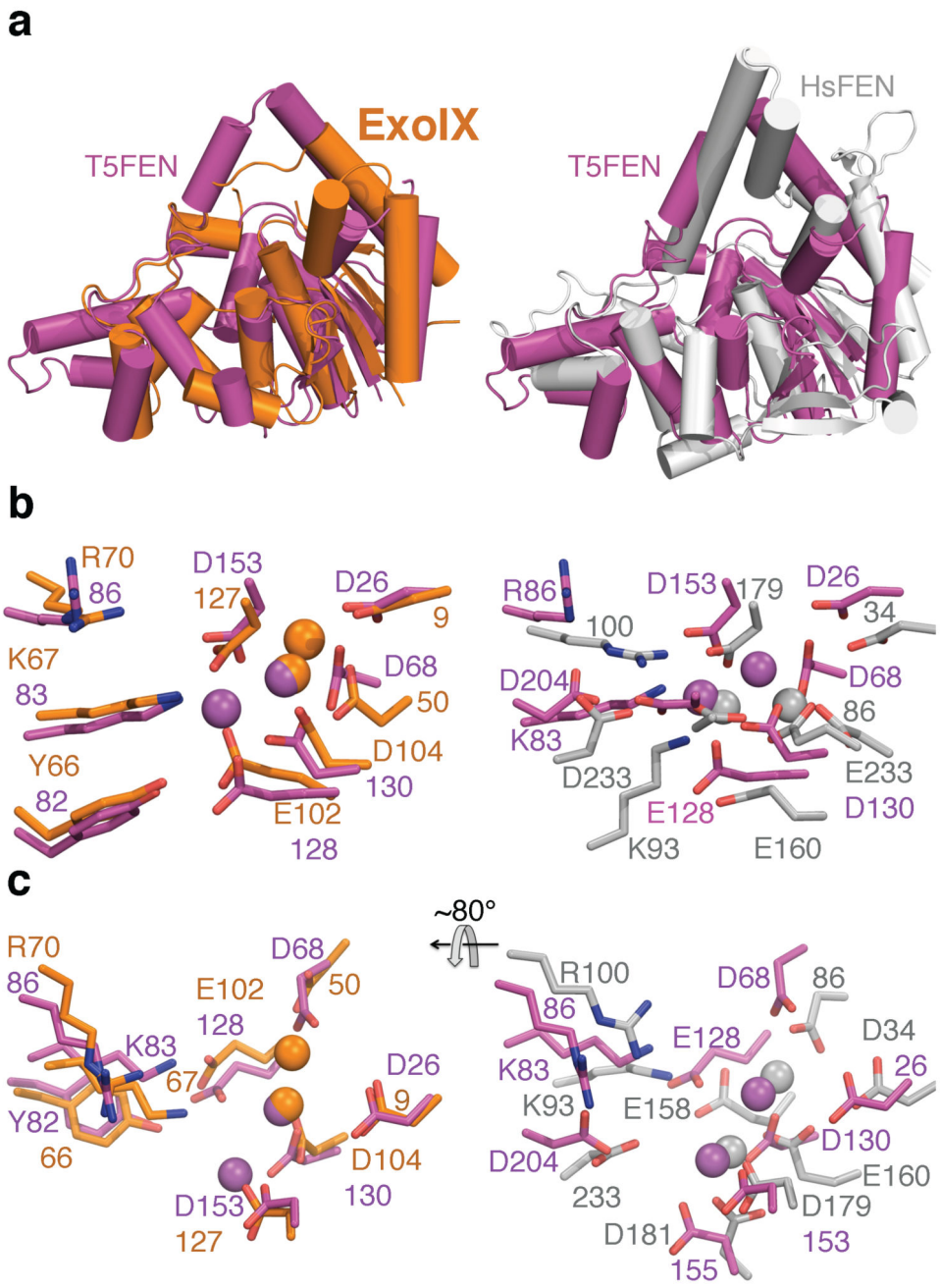


**Figure 6.**

Structural similarities between flap endonucleases. (**a**) Superpositions of T5Fen (magenta cartoons) with *E. coli* ExoIX (orange cartoon) and human FEN (grey cartoon). (**b**,**c**) Views of Cat1 metals (spheres) in T5Fen (magenta sticks) and their ligands superimposed on ExoIX (orange, left panel) and human FEN (grey sticks, right panel).

Europe PMC Funders Author Manuscripts

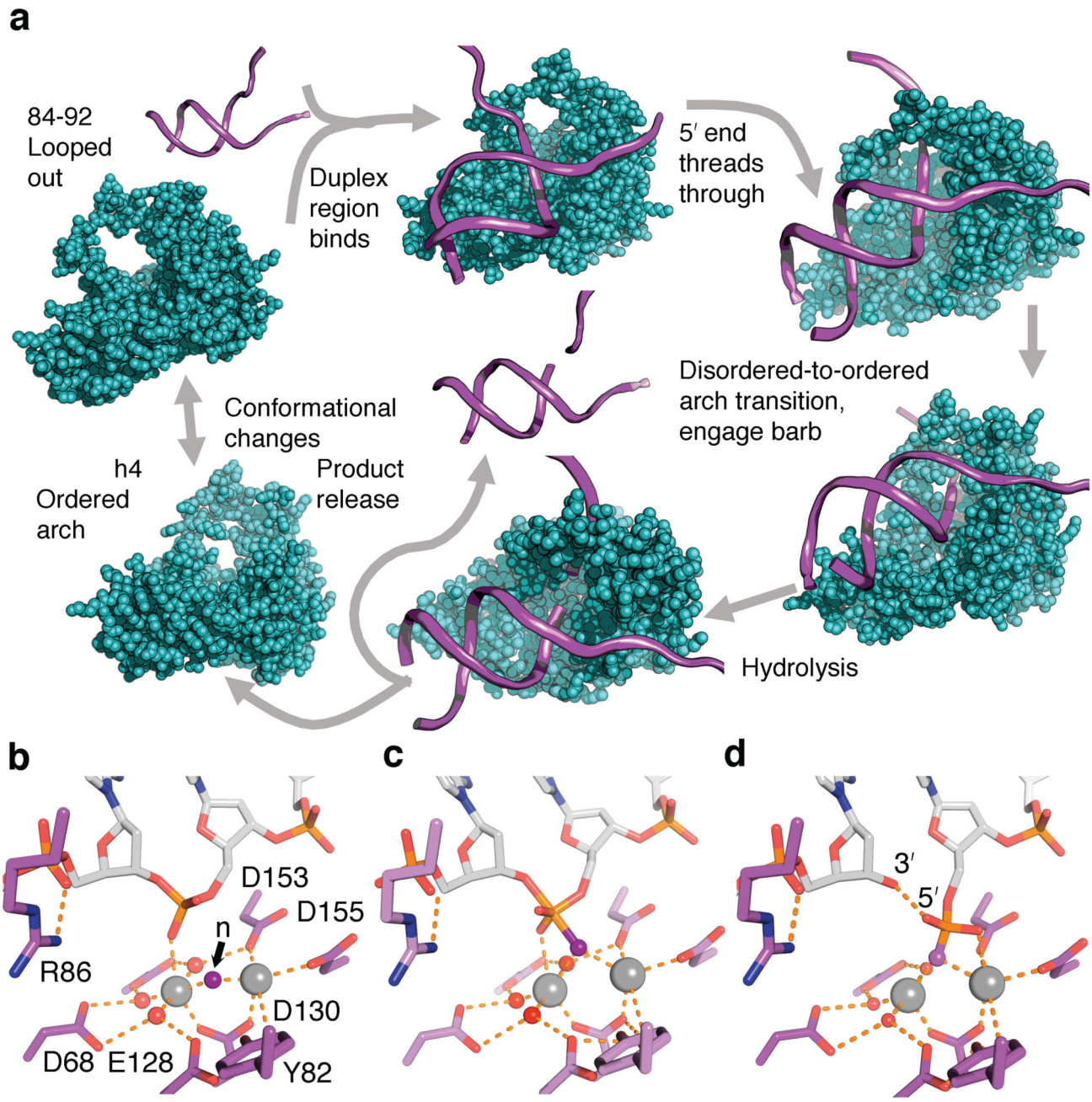


**Figure 7.**

Overview of FEN catalytic cycle. (**a**) Substrate binds disordered conformation (top center). Threading occurs (top right) with ordering of h4, barb engagement followed by hydrolysis and product release. (**b**) Model of active site and scissile nucleotide linkage and water molecule/ $OH^-$ (n, purple sphere) liganded by $Mg^{2+}$ ions (grey spheres). (**c**) Attack of water molecule n on phosphorus generates a trigonal-bipyramidal transition state. (**d**) Products bound in active site.

## Table 1
## Data collection and refinement statistics (molecular replacement)

| | T5Fen (5HMM) | D153K (5HML) | D153K:5ov4 (5HNK) | D155K:3ov6 (5HP4) |
|---|---|---|---|---|
| **Data collection** | | | | |
| Space group | P1 | P1 | $P2_12_12_1$ | $P4_32_12$ |
| Cell dimensions | | | | |
| *a*, *b*, *c* (Å) | 46.8, 58.6, 59.7 | 47.4, 58.4, 59.7 | 44.7, 109.9, 27.3 | 67.5, 67.5, 187.8 |
| *α*,*β*,*γ* (°) | 66.9, 79.4, 73.8 | 66.5, 79.5, 73.7 | 90, 90, 90 | 90, 90, 90 |
| Resolution (Å) [a] | 38.74-1.50 (1.58-1.50) | 54.60-1.48 (1.56-1.48) | 44.72-2.22 (2.28-2.22) | 67.51-1.86 (1.91-1.86) |
| $R_{merge}$ | 0.083 (0.319) | 0.057 (0.491) | 0.079 (0.654) | 0.080 (1.043) |
| $R_{meas}$ | 0.093 (0.438) | 0.069 (0.600) | 0.094 (0.842) | 0.083 (1.079) |
| $R_{pim}$ | 0.042 (0.296) | 0.039 (0.341) | 0.051 (0.521) | 0.022 (0.276) |
| $I/\sigma(I)$ | 10.6 (2.5) | 11.4 (2.2) | 13.4 (2.2) | 30.8 (6.4) |
| Completeness (%) | 93.1 (90.4) | 93.7 (92.6) | 99.4 (94.8) | 99.8 (99.7) |
| Redundancy | 3.8 (2.2) | 3.0 (3.0) | 5.7 (3.1) | 27.9 (28.2) |
| **Refinement** | | | | |
| Resolution (Å) | 38.35-1.50 | 54.60-1.48 | 42.19-2.22 | 54.82-1.86 |
| No. reflections | 79049 | 83074 | 30073 | 35532 |
| $R_{work}$ / $R_{free}$ | 0.147 / 0.196 | 0.141 / 0.196 | 0.187 / 0.234 | 0.169 / 0.196 |
| No. atoms | | | | |
| Protein | 4433 | 4432 | 4407 | 2200 |
| DNA | 0 | 0 | 490 | 345 |
| Ligand/ion | | | | |
| Ethylene glycol | 4 | 8 | | |
| $Mg^{2+}$ | 6 | 3 | 2 | |
| $Cl^-$ | 6 | 13 | | |
| $I^-$ | | 3 | | |
| Bis-Tris propane | | 19 | | |
| Glycerol | | | 6 | 6 |
| $K^+$ | | | 1 | 1 |
| $Ca^{2+}$ | | | | 2 |
| $Na^+$ | | | | 1 |
| Water | 598 | 559 | 224 | 218 |
| *B* factors | | | | |
| Protein | 16.8 | 19.0 | 34.5 | 37.5 |
| DNA | | | 30.8 | 48.8 |
| Ligand/ion | 26.1 | 26.5 | 65.8 | 54.4 |
| Water | 29.5 | 31.3 | 46.7 | 40.0 |
| r.m.s. deviations | | | | |
| Bond lengths (Å) | 0.0105 | 0.0102 | 0.0067 | 0.0102 |

| | T5Fen (5HMM) | D153K (5HML) | D153K:5ov4 (5HNK) | D155K:3ov6 (5HP4) |
|---|---|---|---|---|
| Bond angles (°) | 1.3289 | 1.325 | 1.060 | 1.3714 |

Data from a single crystal was used for each structure determination.

[a]Values in parentheses are for highest-resolution shell.



Europe PMC Funders Author Manuscripts